

Confinement-induced resonances for a two-component ultracold atom gas in arbitrary quasi-one-dimensional traps

V Peano, M Thorwart, C Mora and R Egger

Institut für Theoretische Physik, Heinrich-Heine-Universität Düsseldorf, D-40225
Düsseldorf, Germany

Submitted to: *New J. Phys.*

Abstract. We solve the two-particle s-wave scattering problem for ultracold atom gases confined in arbitrary quasi-one-dimensional trapping potentials, allowing for two different atom species. As a consequence, the center-of-mass and relative degrees of freedom do not factorize. We derive bound-state solutions and obtain the general scattering solution, which exhibits several resonances in the 1D scattering length induced by the confinement. We apply our formalism to two experimentally relevant cases: (i) interspecies scattering in a two-species mixture, and (ii) the two-body problem for a single species in a non-parabolic trap.

PACS numbers: 03.65.Nk, 03.75.Mn, 34.50.-s

1. Introduction

A strongly interacting ultracold atom gas displays interesting features of a correlated quantum many-body system when its dynamics is confined to one dimension [1]. The presence of a transverse confining potential has been shown to induce characteristic resonances in the coupling constant of the two-particle s-wave scattering process [2, 3, 4], which have become known as confinement-induced resonances (CIR). The existence of the CIR has been revealed under the simplifying assumption of a transverse parabolic confinement potential with length scale a_{\perp} and for the case that the two scattering atoms belong to the same species [2, 3, 4]. In this case, the center-of-mass (COM) and relative coordinates of the two particles can be separated, allowing to factorize the problem into single-particle problems. At low temperatures, only the COM ground state is occupied, the decoupled COM motion can be disregarded, and the two-body problem can be solved exactly within the pseudopotential approximation. The result is that there is exactly one bound state for any 3D scattering length a . In the limit of small binding energy, the particles are tightly bound in the lowest-energy transverse state and form a very elongated dimer. The appearance of such a bound state is purely due to the confinement, since for $a < 0$ no dimer is formed in free space. In the opposite limit of large binding energies, the dimer becomes spherically symmetric. In this regime, the confinement is not effective, and the free-space result is recovered. Moreover, a unitary equivalence exists between the Hamiltonian and its projection onto those channels which are perpendicular to the one with lowest energy. As a consequence, to each bound state corresponds a bound state of the closed channels, which then causes the CIR [3]. It occurs at a universal value of the ratio $a_{\perp}/a = \mathcal{C} = -\zeta(1/2, 1) \simeq 1.4603$, where ζ is the Hurvitz zeta function. The influence of the CIR has also been studied for the three-body [5] and the four-body problem [6] in the presence of confinement. In particular, the solution of the four-body problem completely determines the corresponding quasi-1D many-body BCS-BEC crossover phenomenon [6]. Recently, the existence of the confinement-induced molecular bound state in a quasi-1D Fermionic ^{40}K atom gas confined in an optical trap has been reported [7]. By using rf spectroscopy, the binding energy of the dimer has been measured as a function of the scattering length, with quantitative agreement to the results of Ref. [3]. However, the existence of the CIR in the scattering states remains to be observed.

Although the analytical results for the parabolic confinement are instructive, realistic traps for matter waves frequently have non-linear potential forms, see for instance Ref. [8] for a particular example of a trap on the nanometer scale. To give another example, for the problem of tunneling of a macroscopic number of ultracold atoms between two stable states of a trapping potential, the nonlinearity clearly is crucial. Hence generalization to the non-parabolic case is desirable and provided in this work. In addition, we consider traps with two different species of atoms. Note that sympathetic cooling techniques require to study this case. Different trap frequencies may arise for different atom species, e.g., because of different atom masses or different

magnetic quantum numbers. Here we obtain general expressions for the bound-state energies and scattering resonances when the COM and the relative degrees of freedom do not decouple anymore. In the parabolic limit and for intraspecies scattering, we recover well-known results [2, 3]. For the general case, we show that more than one CIR may appear, and that it depends on the symmetry properties of the confining potential how many resonances occur. We apply our formalism to two experimentally relevant cases: (i) interspecies scattering in a two-species mixture of quantum degenerate Bose and Fermi gases in an optical trap, and (ii) a single species cloud in a magnetic trap, taking into account non-parabolic corrections due to a longitudinal magnetic field suppressing Majorana spin flips.

As we will discuss below in more detail, the CIR has a close similarity to the well-known Feshbach resonance [9], which arises if the Hilbert space can be divided into open and closed channels coupled together by a short-range interaction. Due to this small but finite coupling, two incoming particles initially in the open channel visit the closed channels during the scattering process. If a bound state with energy close to the continuum threshold exists, such a process is highly enhanced and a resonance results.

The paper is organized as follows: In Sec. 2, we present the general formalism. Section 3 presents the bound-state solution, while Sec. 4 contains the analysis for the scattering solutions, including the analogy to Feshbach resonances. In Sec. 5 we discuss the special case of harmonic confinement, and in Sec. 6 a particular example of a non-parabolic confinement is illustrated. Finally, we conclude in Sec. 7. Technical details have been delegated to two Appendices. We set $\hbar = 1$ throughout this paper.

2. The two-body problem

Let us consider the general case of two different atomic species with mass m_1 and m_2 . We denote the particle coordinates by $\mathbf{x}_i = (\mathbf{x}_{\perp,i}, z_i)$ and their momenta by $\mathbf{p}_i = (\mathbf{p}_{\perp,i}, p_{\parallel,i})$. Different atoms may experience a different transversal confinement potential $V_i(\mathbf{x}_{\perp,i})$. For ultracold atoms, only low-energy s-wave scattering is relevant, and the interaction between unlike atoms (and similarly, also the interaction between the same atoms) can be described by a Fermi-Huang pseudopotential $V(|\mathbf{x}_1 - \mathbf{x}_2|)$. Then the relevant Hamiltonian for two different atoms is given by

$$H = \frac{\mathbf{p}_1^2}{2m_1} + \frac{\mathbf{p}_2^2}{2m_2} + V_1(\mathbf{x}_{\perp,1}) + V_2(\mathbf{x}_{\perp,2}) + V(|\mathbf{x}_1 - \mathbf{x}_2|). \quad (1)$$

The pseudopotential has the standard form

$$V(\mathbf{r}) = \frac{2\pi a}{\mu} \delta(\mathbf{r}) \frac{\partial}{\partial r} r, \quad (2)$$

where $\mu = m_1 m_2 / (m_1 + m_2)$ is the reduced mass and a the 3D scattering length. This allows to characterize the two-body interaction by the parameter a only. The validity of the pseudopotential approach has been verified numerically for finite-range potentials in Ref. [3]. For further convenience, we transform to the relative/COM coordinates

and momenta given by $\mathbf{r} = (\mathbf{r}_\perp, z)$, $\mathbf{R} = (\mathbf{R}_\perp, Z)$ and $\mathbf{p} = (\mathbf{p}_\perp, p_\parallel)$, $\mathbf{P} = (\mathbf{P}_\perp, P_\parallel)$, respectively. This can be done by the canonical transformation

$$\begin{pmatrix} \mathbf{R} \\ \mathbf{r} \\ \mathbf{P} \\ \mathbf{p} \end{pmatrix} = \frac{1}{M} \begin{pmatrix} m_1 & m_2 & 0 & 0 \\ M & -M & 0 & 0 \\ 0 & 0 & M & M \\ 0 & 0 & m_2 & -m_1 \end{pmatrix} \begin{pmatrix} \mathbf{x}_1 \\ \mathbf{x}_2 \\ \mathbf{p}_1 \\ \mathbf{p}_2 \end{pmatrix}, \quad (3)$$

where $M = m_1 + m_2$. Since the confinement is assumed to be purely transversal, the longitudinal COM coordinate Z is free and decouples from the other degrees of freedom. Hence we eliminate it by transforming into the longitudinal COM rest frame, where the state $|\Psi\rangle$ of the system is determined by the set of coordinates $(\mathbf{x}_{\perp,1}, \mathbf{x}_{\perp,2}, z)$ or, alternatively, by $(\mathbf{R}_\perp, \mathbf{r}) = (\mathbf{R}_\perp, \mathbf{r}_\perp, z)$. The transformed Hamiltonian takes the form

$$H = H_\parallel + H_{\perp,1} + H_{\perp,2} + V, \quad (4)$$

where

$$H_\parallel = \frac{p_\parallel^2}{2\mu}, \quad H_{\perp,i} = \frac{\mathbf{p}_{\perp,i}^2}{2m_i} + V_i(\mathbf{x}_{\perp,i}). \quad (5)$$

For a more compact notation, we introduce the non-interacting Hamiltonian $H_0 = H - V$ and denote its eigenstates by

$$|k, \lambda_1, \lambda_2\rangle = e^{-ikz} \psi_{\lambda_1}^{(1)}(\mathbf{x}_{\perp,1}) \psi_{\lambda_2}^{(2)}(\mathbf{x}_{\perp,2}), \quad (6)$$

where $\psi_{\lambda_i}^{(i)}$ are single-particle eigenstates of $H_{\perp,i}$ for eigenvalue $E_{\lambda_i}^{(i)}$. Correspondingly, the two-particle Schrödinger equation is given by

$$(H_0 - E) \Psi(\mathbf{R}_\perp, \mathbf{r}) = -V(\mathbf{r}) \Psi(\mathbf{R}_\perp, \mathbf{r}). \quad (7)$$

The pseudopotential (2) can be enforced by the Bethe-Peierls boundary condition

$$\Psi(\mathbf{R}_\perp, \mathbf{r} \rightarrow 0) \simeq \frac{f(\mathbf{R}_\perp)}{4\pi r} \left(1 - \frac{r}{a}\right), \quad (8)$$

leading to the inhomogeneous Schrödinger equation

$$(H_0 - E) \Psi(\mathbf{R}_\perp, \mathbf{r}) = \frac{f(\mathbf{R}_\perp)}{2\mu} \delta(\mathbf{r}). \quad (9)$$

The solution of this equation can be formally obtained in terms of a solution of the homogeneous Schrödinger equation, $(H_0 - E)\Psi_0 = 0$, and the Green's function $G_E = (H_0 - E)^{-1}$,

$$\Psi(\mathbf{R}_\perp, \mathbf{r}) = \Psi_0(\mathbf{R}_\perp, \mathbf{r}) + \int d\mathbf{R}'_\perp G_E(\mathbf{R}_\perp, \mathbf{r}; \mathbf{R}'_\perp, 0) \frac{f(\mathbf{R}'_\perp)}{2\mu}. \quad (10)$$

To determine $f(\mathbf{R}_\perp)$, we substitute Eq. (10) into Eq. (8) and find the integral equation

$$-\frac{f(\mathbf{R}_\perp)}{4\pi a} = \Psi_0(\mathbf{R}_\perp, 0) + \int d\mathbf{R}'_\perp \zeta_E(\mathbf{R}_\perp, \mathbf{R}'_\perp) f(\mathbf{R}'_\perp), \quad (11)$$

where we have defined the regularized integral kernel

$$\zeta_E(\mathbf{R}_\perp, \mathbf{R}'_\perp) = \lim_{r \rightarrow 0} \frac{1}{2\mu} \left(G_E(\mathbf{R}_\perp, \mathbf{r}; \mathbf{R}'_\perp, 0) - \delta(\mathbf{R}_\perp - \mathbf{R}'_\perp) \frac{\mu}{2\pi r} \right). \quad (12)$$

In Eqs. (10) and (11), Ψ_0 can be expressed as a superposition of single-particle eigenstates $|k, \lambda_1, \lambda_2\rangle$ with

$$\frac{k^2}{2\mu} + E_{\lambda_1}^{(1)} + E_{\lambda_2}^{(2)} = E. \quad (13)$$

We refer to the set of states with the same transverse occupation numbers λ_i but arbitrary longitudinal relative momentum as a *scattering channel* or, simply, *channel*. Each channel has a minimum energy given by $E_{\lambda_1}^{(1)} + E_{\lambda_2}^{(2)}$. Since the interaction is short-ranged, only states fulfilling Eq. (13) appear in the asymptotic solution. For each *open channel*, $E > E_{\lambda_1}^{(1)} + E_{\lambda_2}^{(2)}$, such that there are (at least) two such states having opposite momenta. For E just above $E_0^{(1)} + E_0^{(2)}$, there exists one open channel only. The corresponding solution given by Eq. (10) describes the scattering of two particles initially occupying the transverse ground-state. During the scattering process, the particles populate closed channels, but afterwards return into the single available open channel (quasi-1D picture). For $E < E_0^{(1)} + E_0^{(2)}$, all channels are closed and only bound-state solutions are possible. These are given by Eq. (10) with $\Psi_0(\mathbf{R}_\perp, \mathbf{r}) = 0$. In the following, we consider both classes of solutions in more detail.

3. Bound-state solutions

Let us consider the situation when all channels are closed and only bound states may occur. We define the binding energy of the bound states as

$$E_B = E_0 - E > 0, \quad (14)$$

where $E_0 = E_0^{(1)} + E_0^{(2)}$ is the ground-state energy of H_0 . To find bound states, we diagonalize the operator $\zeta_E(\mathbf{R}_\perp, \mathbf{R}'_\perp)$ defined in Eq. (12), where Eq. (11) yields the condition

$$-\frac{f(\mathbf{R}_\perp)}{4\pi a} = \int d\mathbf{R}'_\perp \zeta_E(\mathbf{R}_\perp, \mathbf{R}'_\perp) f(\mathbf{R}'_\perp). \quad (15)$$

For given a , bound states with binding energy $E_B = E_0 - E$ follow as solution of this eigenvalue problem. The bound-state wave function follows by inserting the corresponding eigenvector $f(\mathbf{R}_\perp)$ into Eq. (10) with $\Psi_0(\mathbf{R}_\perp, \mathbf{r}) = 0$. In order to find a representation of $\zeta_E(\mathbf{R}_\perp, \mathbf{R}'_\perp)$ allowing for straightforward analytical or numerical diagonalization, we use

$$G_E(\mathbf{R}_\perp, \mathbf{r}; \mathbf{R}'_\perp, 0) = \int_0^\infty dt e^{Et} G_t(\mathbf{R}_\perp, \mathbf{r}; \mathbf{R}'_\perp, 0), \quad (16)$$

with the imaginary-time evolution operator

$$G_t(\mathbf{R}_\perp, \mathbf{r}; \mathbf{R}'_\perp, 0) = \langle \mathbf{R}_\perp, \mathbf{r} | \exp[-H_0 t] | \mathbf{R}'_\perp, 0 \rangle \quad (17)$$

for H_0 . The time evolution operator $\exp[-H_0 t]$ can be factorized into the product $\exp[-H_\parallel t] \exp[-H_{1,\perp} t] \exp[-H_{2,\perp} t]$. The corresponding factors in G_t are

$$\langle z | \exp[-H_\parallel t] | z' \rangle = \left(\frac{\mu}{2\pi t} \right)^{1/2} e^{-(z-z')^2 \mu/2t} \quad (18)$$

for the relative longitudinal coordinates and

$$\langle \mathbf{x}_{i,\perp} | \exp[-H_{i,\perp}t] | \mathbf{x}'_{i,\perp} \rangle = \sum_{\lambda} e^{-E_{\lambda}^{(i)}t} \psi_{\lambda}^{(i)}(\mathbf{x}_{i,\perp}) \bar{\psi}_{\lambda}^{(i)}(\mathbf{x}'_{i,\perp}) \quad (19)$$

for the transverse coordinates (the bar denotes complex conjugation). Thus G_t can be expressed in terms of the set of coordinates $(\mathbf{x}_{\perp,1}, \mathbf{x}_{\perp,2}, z)$ as

$$G_t(\mathbf{R}_{\perp}, \mathbf{r}; \mathbf{R}'_{\perp}, 0) = \sqrt{\frac{\mu}{2\pi t}} e^{-z^2\mu/2t} \prod_{i=1,2} \sum_{\lambda} e^{-E_{\lambda}^{(i)}t} \psi_{\lambda}^{(i)}(\mathbf{x}_{\perp,i}) \bar{\psi}_{\lambda}^{(i)}(\mathbf{x}'_{\perp,i}). \quad (20)$$

This equation illustrates that for large imaginary times the integrand in Eq. (16) decays as $\exp[-E_B t]$. Notice that this representation is valid for $E_B > 0$. By using

$$\frac{\mu}{2\pi r} = \int_0^{\infty} dt \left(\frac{\mu}{2\pi t} \right)^{3/2} e^{-r^2\mu/2t} \quad (21)$$

we find

$$\zeta_E(\mathbf{R}_{\perp}, \mathbf{R}'_{\perp}) = \int_0^{\infty} \frac{dt}{2\mu} \left[e^{Et} G_t(\mathbf{R}_{\perp}, 0; \mathbf{R}'_{\perp}, 0) - \left(\frac{\mu}{2\pi t} \right)^{3/2} \delta(\mathbf{R}_{\perp} - \mathbf{R}'_{\perp}) \right]. \quad (22)$$

To show that the integral in Eq. (22) converges also for small t , we expand $G_t(\mathbf{R}_{\perp}, 0; \mathbf{R}'_{\perp}, 0)$ with respect to t , see Appendix A. We find

$$\begin{aligned} \lim_{t \rightarrow 0} G_t(\mathbf{R}_{\perp}, 0; \mathbf{R}'_{\perp}, 0) &= \left(\frac{\mu}{2\pi t} \right)^{3/2} \delta(\mathbf{R}_{\perp} - \mathbf{R}'_{\perp}) - t^{-1/2} \left(\frac{\mu}{2\pi} \right)^{3/2} \\ &\quad \times \left[\frac{\mathbf{P}_{\perp}^2}{2M} + V_1(\mathbf{R}_{\perp}) + V_2(\mathbf{R}_{\perp}) \right]. \end{aligned} \quad (23)$$

Thus ζ_E can be regarded as a regular operator acting on the space \mathcal{L}^2 of square-integrable functions. We note in passing that if the two single-particle transverse Hamiltonians $H_{\perp,i}$ commute with the angular momentum operators L_z , then also ζ_E commutes with L_z . This follows by observing that in this case we can choose for the eigenbasis $\{\psi_{\lambda}^{(i)}\}$ a set of eigenvectors of L_z , and the product of two eigenvectors of L_z is still an eigenvector of L_z . Hence $\zeta_E(\mathbf{R}_{\perp}, \mathbf{R}'_{\perp})$ can be written as a sum of projectors onto states with definite angular momentum. A similar conclusion can be drawn regarding parity symmetry, when considering non-cylindrical confining potentials that obey this symmetry.

Using the transverse non-interacting ground state,

$$\psi_0(\mathbf{R}_{\perp}, \mathbf{r}_{\perp}) = \psi_0^{(1)} \left(\mathbf{R}_{\perp} + \frac{\mu}{m_1} \mathbf{r}_{\perp} \right) \psi_0^{(2)} \left(\mathbf{R}_{\perp} - \frac{\mu}{m_2} \mathbf{r}_{\perp} \right), \quad (24)$$

provided the overlap integral $\int d\mathbf{R}'_{\perp} \bar{\psi}_0(\mathbf{R}'_{\perp}, 0) f(\mathbf{R}'_{\perp}) \neq 0$, the integrand in Eq. (10) decays as $\exp[-E_B t]$. This defines a spatial scale a_B for the longitudinal size of the corresponding bound state, $a_B = 1/\sqrt{\mu E_B}$. For large E_B , a_B is small and we have very tight pairs. This constitutes the *dimer limit*. On the other hand, for small E_B , atom pairs are very elongated. This regime is termed *BCS limit*. In the following, we investigate both limits in greater detail.

3.1. Dimer limit

For large binding energies, the atom-atom interaction dominates over the confinement. Due to the exponential factors in Eq. (22), only small imaginary times contribute significantly to the integral, and we can substitute G_t with the short-time expansion (23) as derived in the Appendix A, yielding

$$\zeta_E(\mathbf{R}_\perp, \mathbf{R}'_\perp) \simeq \left(\frac{\mu}{2\pi}\right)^{3/2} \int_0^\infty \frac{dt}{2\mu} (t^{-3/2} (e^{Et} - 1) \delta(\mathbf{R}_\perp - \mathbf{R}'_\perp) - e^{Et} t^{-1/2} \langle \mathbf{R}_\perp | H_\perp | \mathbf{R}'_\perp \rangle) . \quad (25)$$

Hence, the operator ζ_E now shares eigenfunctions with $H_\perp = \mathbf{P}_\perp^2/2M + V_1(\mathbf{R}_\perp) + V_2(\mathbf{R}_\perp)$. For (identical) parabolic confinement potentials, H_\perp is exactly the decoupled COM Hamiltonian. Let us denote the eigenfunctions and eigenenergies of H_\perp as $\phi_\lambda(\mathbf{R}_\perp)$ and $E_\lambda^{(\phi)}$, respectively. Substituting $\phi_\lambda(\mathbf{R}_\perp)$ into Eq. (15) yields after some algebra

$$-\frac{1}{4\pi a} = -\frac{\sqrt{2\mu|E|}}{4\pi} \left(1 + \frac{E_\lambda^{(\phi)}}{2|E|}\right) \simeq -\frac{\sqrt{2\mu E_B}}{4\pi} . \quad (26)$$

In the second relation, we have used Eq. (14). From this, we directly obtain the binding energy in the dimer limit $a \rightarrow 0^+$ as

$$E_B \approx \frac{1}{2\mu a^2} , \quad (27)$$

which coincides with the result obtained in free (3D) space without confinement.

3.2. BCS limit

The scattering channel with lowest energy, corresponding to the transverse non-interacting ground state ψ_0 , opens at the energy threshold $E = E_0$. For $E_B \rightarrow 0^+$, as the energy approaches this threshold, the term with $\lambda_1 = \lambda_2 = 0$ dominates in Eq. (20), and yields in Eq. (22) the contribution

$$\sqrt{\frac{1}{8\mu E_B}} \psi_0(\mathbf{R}_\perp, 0) \bar{\psi}_0(\mathbf{R}'_\perp, 0) , \quad (28)$$

which diverges for $E_B \rightarrow 0^+$. All other channels are still closed at $E = E_0$ and give finite contributions in Eq. (20). This observation suggests a useful separation of the total Hilbert space into a part \mathcal{H}_o corresponding to the open channel (or lowest-energy scattering channel) and a part \mathcal{H}_e perpendicular to that. With this separation, terms yielding a finite contribution at $E_B \rightarrow 0^+$ can be summarized in the Green's function

$$\tilde{G}_t(\mathbf{R}_\perp, \mathbf{r}; \mathbf{R}'_\perp, 0) = \langle \mathbf{R}_\perp, \mathbf{r} | \exp[-\tilde{H}_0 t] | \mathbf{R}'_\perp, 0 \rangle , \quad (29)$$

where \tilde{H}_0 is the projection of H_0 onto the Hilbert subspace \mathcal{H}_e . We then define a new integral kernel,

$$\tilde{\zeta}_E(\mathbf{R}_\perp, \mathbf{R}'_\perp) = \int_0^\infty \frac{dt}{2\mu} \left[e^{Et} \tilde{G}_t(\mathbf{R}_\perp, 0; \mathbf{R}'_\perp, 0) - \left(\frac{\mu}{2\pi t}\right)^{3/2} \delta(\mathbf{R}_\perp - \mathbf{R}'_\perp) \right] , \quad (30)$$

which is also well-defined for energies above the threshold $E = E_0$.

For small E_B , Eq. (15) is most conveniently solved by expanding $f(\mathbf{R}_\perp)$ in an orthonormal basis $|j\rangle$ according to

$$|f\rangle = \sum_j f_j |j\rangle, \quad f_j = \int d\mathbf{R}_\perp \langle j|\mathbf{R}_\perp\rangle f(\mathbf{R}_\perp), \quad (31)$$

where the basis state $|0\rangle$ corresponds to

$$\langle \mathbf{R}_\perp | 0 \rangle = c\psi_0(\mathbf{R}_\perp, 0), \quad (32)$$

with normalization constant c . Although $\psi_0(\mathbf{R}_\perp, \mathbf{r})$ is a normalized element of the two-particle Hilbert space, this does not imply that $\psi_0(\mathbf{R}_\perp, 0)$ is an element of the COM Hilbert space with norm unity. In fact, the normalization constant c has to be computed explicitly and generally depends on the particular confinement. In this basis, Eq. (15) assumes the compact form

$$-\frac{|f\rangle}{4\pi a} = \zeta_E |f\rangle = \left(\sqrt{\frac{1}{8\mu E_B}} \frac{|0\rangle\langle 0|}{c^2} + \tilde{\zeta}_E \right) |f\rangle. \quad (33)$$

$|0\rangle$ is an approximate eigenstate for small E_B , since all the matrix elements are finite apart from $\langle 0|\zeta_E|0\rangle$ which diverges according to

$$\langle 0|\zeta_E|0\rangle \simeq \sqrt{\frac{1}{8\mu E_B}} \frac{1}{c^2} + \langle 0|\tilde{\zeta}_E|0\rangle. \quad (34)$$

Substituting this in Eq. (33) yields

$$-\frac{1}{4\pi a} \simeq \sqrt{\frac{1}{8\mu E_B}} \frac{1}{c^2} + \langle 0|\tilde{\zeta}_E|0\rangle. \quad (35)$$

Neglecting the last term, the relation for the binding energy E_B is solved in the BCS limit $a \rightarrow 0^-$,

$$E_B \approx \frac{2a^2\pi^2}{\mu c^4}. \quad (36)$$

4. Scattering solutions

In this section, we focus on scattering solutions at low energies E slightly above E_0 , where exactly one transverse channel is open. Then the incoming state is given by

$$\Psi_0 = e^{ikz} \psi_0^{(1)}(\mathbf{x}_{1,\perp}) \psi_0^{(2)}(\mathbf{x}_{2,\perp}), \quad (37)$$

which describes two incoming atoms with (small) relative longitudinal momentum $k = \sqrt{2m(E - E_0)}$ in the (transverse) single-particle ground states $\psi_0^{(1)}$ and $\psi_0^{(2)}$, respectively.

4.1. One-dimensional scattering length a_{1D}

As done in Sec. 3, we split off the contribution from the open channel,

$$G_E(\mathbf{R}_\perp, \mathbf{r}; \mathbf{R}'_\perp, 0) = \psi_0(\mathbf{R}_\perp, \mathbf{r}_\perp) \bar{\psi}_0(\mathbf{R}'_\perp, 0) \frac{i\mu}{k} e^{ik|z|} + \int_0^\infty dt e^{Et} \tilde{G}_t(\mathbf{R}_\perp, \mathbf{r}; \mathbf{R}'_\perp, 0), \quad (38)$$

where $\tilde{G}_t(\mathbf{R}_\perp, z; \mathbf{R}'_\perp, 0)$ is the Green's function restricted to \mathcal{H}_e , which is well-defined also above E_0 . Inserting Eq. (38) into Eq. (10) yields for $|z| \rightarrow \infty$ the standard scattering solution,

$$\Psi(\mathbf{R}, \mathbf{r}) = \psi_0(\mathbf{R}_\perp, \mathbf{r}_\perp) (e^{ikz} + f_e(k) e^{ik|z|}), \quad (39)$$

with scattering amplitude

$$f_e(k) = \frac{i}{2k} \int d\mathbf{R}'_\perp \bar{\psi}_0(\mathbf{R}'_\perp, 0) f(\mathbf{R}'_\perp), \quad (40)$$

whereas for short distances, also the term $\int d\mathbf{R}'_\perp \int_0^\infty dt e^{Et} \tilde{G}_t(\mathbf{R}_\perp, \mathbf{r}; \mathbf{R}'_\perp, 0) f(\mathbf{R}'_\perp)$ appears in the scattering solution. Since the energy is well below the continuum threshold for the closed channels, this must be regarded as a sum over localized states. Enforcing the boundary condition (8) then leads to an integral equation for $f(\mathbf{R}_\perp)$,

$$-\frac{f(\mathbf{R}_\perp)}{4\pi a} = \int d\mathbf{R}'_\perp \tilde{\zeta}_E(\mathbf{R}_\perp, \mathbf{R}'_\perp) f(\mathbf{R}'_\perp) + \psi_0(\mathbf{R}_\perp, 0) + \frac{i\psi_0(\mathbf{R}_\perp, 0)}{2k} \int d\mathbf{R}'_\perp \bar{\psi}_0(\mathbf{R}'_\perp, 0) f(\mathbf{R}'_\perp). \quad (41)$$

This integral equation is most conveniently solved by again expanding $f(\mathbf{R}_\perp)$ in the orthonormal basis $\{|j\rangle\}$ introduced in the previous section. Thereby, we can express Eq. (41) in compact notation,

$$-\frac{|f\rangle}{4\pi a} = \frac{|0\rangle}{c} + \frac{i}{2k} \frac{|0\rangle}{c^2} \langle 0|f\rangle + \tilde{\zeta}_E|f\rangle, \quad (42)$$

which is formally solved by

$$|f\rangle = \frac{-1/c}{1 - i/(ka_{1D})} \left(\tilde{\zeta}_E + \frac{1}{4\pi a} \right)^{-1} |0\rangle. \quad (43)$$

The parameter a_{1D} follows in the form

$$a_{1D} = -\frac{2c^2}{\langle 0|[\tilde{\zeta}_E + 1/(4\pi a)]^{-1}|0\rangle}. \quad (44)$$

From Eq. (40), $f_e(k) = -1/(1 + ika_{1D})$, which allows to identify a_{1D} with the *1D scattering length*. Having introduced this parameter, the 1D atom-atom interaction potential can then be written in an effective form according to

$$V_{1D}(z, z') = g_{1D} \delta(z - z'), \quad (45)$$

with interaction strength $g_{1D} = -1/(\mu a_{1D})$ [2]. For very low energies, $k \rightarrow 0$, we can now formally set $E = E_0$ in Eq. (44). For a confining trap, $\tilde{\zeta}_{E_0}$ is a Hermitian operator with

discrete spectrum $\{\lambda_n\}$ and eigenvectors $|e_n\rangle$, which eventually have to be determined for the particular Hamiltonian. Thus we find

$$g_{1D} = \frac{1}{2\mu c^2} \sum_n \frac{|\langle 0|e_n\rangle|^2}{\lambda_n + 1/(4\pi a)}. \quad (46)$$

This result has interesting consequences for the two-body interaction. The denominator can become singular for particular values of a , thereby generating a CIR. Every eigenvalue λ_n corresponds to a different CIR, unless the overlap $\langle 0|e_n\rangle$ vanishes due to some underlying symmetry of the Hamiltonian. We anticipate that for identical parabolic confinement potentials, the decoupling of the COM motion implies that only one resonance is permitted. For confining potentials with cylindrical symmetry, there is a resonance for each eigenvector of $\tilde{\zeta}_{E_0}$ with zero angular momentum. For confining potentials obeying parity symmetry, the eigenstates $|e_n\rangle$ must be even. These two symmetries allow in principle for infinitely many resonances. In practice, however, only few of them can be resolved because the resonances become increasingly sharper when $|\langle 0|e_n\rangle|^2 \rightarrow 0$, making them difficult to detect.

4.2. Interpretation of the CIR as Feshbach resonances

A very simple and illuminating analysis, similar to that for standard Feshbach resonances [9], is also possible for the CIR. The two-particle Schrödinger equation can be rewritten as an effective Schrödinger equation for the scattering states in the open channel, $(E - H_{\text{eff}})\mathcal{P}|\Psi\rangle = 0$, with the effective Hamiltonian

$$H_{\text{eff}} = H_{\text{open}} + \mathcal{P}H\mathcal{M} \frac{1}{E - H_{\text{closed}}} \mathcal{M}H\mathcal{P}. \quad (47)$$

Here, $H_{\text{open}} = \mathcal{P}H\mathcal{P}$ and $H_{\text{closed}} = \mathcal{M}H\mathcal{M}$, where \mathcal{P} and \mathcal{M} are projectors to open and closed channels, respectively. This equation can be expressed in terms of the closed-channel eigenstates $|\Phi_n\rangle$,

$$H_{\text{eff}} = H_{\text{open}} + \mathcal{P}H \sum_n \frac{|\Phi_n\rangle\langle\Phi_n|}{E - E_n} H\mathcal{P}, \quad (48)$$

with $H_{\text{closed}}|\Phi_n\rangle = E_n|\Phi_n\rangle$. This implies that a Feshbach-like resonance is possible at zero momentum if two conditions are fulfilled. First, there exists a solution of $(E_0 - H_{\text{closed}})|\Phi\rangle = 0$, i.e., $|\Phi\rangle$ is a bound state of H_{closed} with energy $E = E_0$. Second, $|\Phi\rangle$ must be coupled to the open channel, $\mathcal{P}H|\Phi\rangle \neq 0$.

Within the pseudopotential approximation, the equation $(E_0 - H_{\text{closed}})|\Phi\rangle = 0$ is solved in terms of the Green's function

$$\mathcal{M}G_{E_0}(\mathbf{R}_\perp, \mathbf{r}; \mathbf{R}'_\perp, 0)\mathcal{M} = \int_0^\infty dt e^{E_0 t} \tilde{G}_t(\mathbf{R}_\perp, \mathbf{r}; \mathbf{R}'_\perp, 0) \quad (49)$$

by the state

$$\Phi(\mathbf{R}_\perp, \mathbf{r}) = \int d\mathbf{R}'_\perp \mathcal{M}G_{E_0}(\mathbf{R}_\perp, \mathbf{r}; \mathbf{R}'_\perp, 0)\mathcal{M} \frac{f(\mathbf{R}'_\perp)}{2\mu}, \quad (50)$$

together with boundary condition

$$\Phi(\mathbf{R}_\perp, \mathbf{r} \rightarrow 0) \simeq \frac{f(\mathbf{R}_\perp)}{4\pi r} \left(1 - \frac{r}{a}\right). \quad (51)$$

This leads to the eigenvalue equation

$$-\frac{|f\rangle}{4\pi a} = \tilde{\zeta}_{E_0}|f\rangle, \quad (52)$$

which is solved by the eigenvectors $|e_n\rangle$ introduced above. This yields $a = -1/(4\pi\lambda_n)$, implying that there is a bound state $|\Phi\rangle$ of H_{closed} with energy equal to the energy of the incoming wave, corresponding to the resonances found in the previous subsection. The CIR is then in complete analogy to a zero-momentum Feshbach resonance. Due to the small but finite coupling to the closed channels, two incoming particles initially in the open channel visit the closed channels during the scattering process. This process is strongly intensified when a bound-state exists whose energy is close to the continuum threshold. Then, a scattering resonance results. Note that such a bound state can be occupied only virtually by two particles during the scattering process. Hence from now on we will refer to such a bound state as a virtual bound state.

It is also possible to recover the overlap condition $\langle 0|e_n\rangle \neq 0$ in this framework. In fact,

$$\mathcal{P}H\Phi(\mathbf{R}_\perp, \mathbf{r}) = \mathcal{P}V(\mathbf{r})\Phi(\mathbf{R}_\perp, \mathbf{r}) = -\mathcal{P}\frac{\langle \mathbf{R}_\perp|e_n\rangle}{2\mu}\delta(\mathbf{r}) = -\psi_0(\mathbf{R}_\perp, \mathbf{r}_\perp)\delta(z)\frac{\langle 0|e_n\rangle}{2\mu c}, \quad (53)$$

since $|\Phi\rangle$ fulfills Eq. (51) with $f(\mathbf{R}) = \langle \mathbf{R}_\perp|e_n\rangle$. Hence, the two overlap conditions

$$\mathcal{P}H|\Phi\rangle \neq 0 \quad \Leftrightarrow \quad \langle 0|e_n\rangle \neq 0 \quad (54)$$

are equivalent. When they are not fulfilled, there exists a virtual bound state with energy E_0 , but it is not coupled to the incoming wave.

5. Special case of harmonic confinement

In the previous sections, we have formulated the theory for a general confining potential and for two different atomic species. As a simple illustration, we now consider the case of harmonic confinement, $V_i(\mathbf{x}_i) = m_i\omega_i^2\mathbf{x}_{i\perp}^2/2$. In COM and relative coordinates,

$$\begin{aligned} V_{\text{conf}}(\mathbf{R}_\perp, \mathbf{r}_\perp) &= \frac{1}{2}(m_1\omega_1^2 + m_2\omega_2^2)|\mathbf{R}_\perp|^2 + \frac{1}{2}\left(\frac{\mu^2}{m_1}\omega_1^2 + \frac{\mu^2}{m_2}\omega_2^2\right)|\mathbf{r}_\perp|^2 \\ &\quad + \mu(\omega_1^2 - \omega_2^2)\mathbf{r}_\perp \cdot \mathbf{R}_\perp. \end{aligned} \quad (55)$$

In general, the COM and the relative coordinate do not decouple, and in order to find the scattering and bound-state solutions, we have to follow the procedure outlined in the previous sections. To that end, we label the single-particle transverse states by quantum numbers $\lambda = \{m, n\}$, where m is the integer angular momentum and n the integer radial quantum number. The eigenenergies and -states of the 2D harmonic oscillator

$$E_\lambda^{(i)} = \omega_i \epsilon_{n,m}, \quad \psi_\lambda^{(i)} = \frac{1}{a_i} \psi_{n,m} \left(\frac{\mathbf{x}_\perp}{a_i} \right),$$

with the oscillator lengths $a_i = (m_i \omega_i)^{-1/2}$, $i = 1, 2$, can be expressed in terms of the quantities

$$\epsilon_{n,m} = 2n + |m| + 1 \quad \text{and} \quad \psi_{n,m}(\mathbf{x}_\perp) = e^{im\phi} R_{n,m}(|\mathbf{x}_\perp|),$$

where

$$R_{n,m}(\rho) = \frac{1}{\sqrt{\pi}} \left(\frac{n!}{(n + |m|)!} \right)^{1/2} e^{-\rho/2} \rho^{|m|} L_n^{|m|}(\rho^2),$$

with $L_n^{|m|}(x)$ being the standard Laguerre polynomials. A convenient choice for the orthonormal basis $|j\rangle$ introduced in Eq. (31) is then given by

$$\langle \mathbf{R}_\perp | j \rangle = \langle \mathbf{R}_\perp | m, n \rangle = \frac{1}{a_M} \psi_{n,m} \left(\frac{|\mathbf{R}_\perp|}{a_M} \right), \quad (56)$$

with the length scale $a_M = (m_1 \omega_1 + m_2 \omega_2)^{-1/2}$. In particular, we find for $|0\rangle = |0, 0\rangle$ that $\langle \mathbf{R}_\perp | 0 \rangle$ fulfills Eq. (32) with $c = \sqrt{\pi} a_1 a_2 / a_M$.

The single-particle imaginary-time propagator for a 2D harmonic oscillator with length scale a_0 and frequency ω is given by

$$\sum_\lambda e^{-\omega \epsilon_\lambda t} \frac{1}{a_0^2} \psi_\lambda \left(\frac{\mathbf{x}_\perp}{a_0} \right) \bar{\psi}_\lambda \left(\frac{\mathbf{x}'_\perp}{a_0} \right) = \frac{1}{\pi a_0^2} \frac{e^{-\omega t}}{1 - e^{-2\omega t}} \exp \left[-\frac{\mathbf{x}_\perp^2 + \mathbf{x}'_\perp{}^2}{2a_0^2} \coth(\omega t) + \frac{\mathbf{x}_\perp \cdot \mathbf{x}'_\perp}{a_0^2 \sinh(\omega t)} \right]. \quad (57)$$

Inserting this into Eq. (20) with $\mathbf{x}_{\perp,i} = \mathbf{R}_\perp$, $\mathbf{x}'_{\perp,i} = \mathbf{R}'_\perp$ and $z = 0$, we find

$$G_t(\mathbf{R}_\perp, 0; \mathbf{R}'_\perp, 0) = \sqrt{\frac{\mu}{2\pi t}} \frac{\beta(1-\beta)}{\pi^2 a_M^4} \frac{e^{-\omega_1 t}}{1 - e^{-2\omega_1 t}} \frac{e^{-\omega_2 t}}{1 - e^{-2\omega_2 t}} \times \exp \left[-\frac{\mathbf{R}_\perp^2 + \mathbf{R}'_\perp{}^2}{2a_M^2} f(t) + \frac{\mathbf{R}_\perp \cdot \mathbf{R}'_\perp}{a_M^2} g(t) \right], \quad (58)$$

where we have introduced $\beta = a_M^2 / a_1^2$ and

$$\begin{aligned} f(t) &= \beta \coth(\omega_1 t) + (1 - \beta) \coth(\omega_2 t), \\ g(t) &= \beta \sinh^{-1}(\omega_1 t) + (1 - \beta) \sinh^{-1}(\omega_2 t). \end{aligned} \quad (59)$$

In order to compute explicitly the operators ζ_E and $\tilde{\zeta}_E$, we still have to project onto the discrete basis $\{|j\rangle\}$ and to perform the imaginary-time integral for each matrix element. In general, this cannot be achieved analytically, and one has to resort to a numerical evaluation. Only for $\omega_1 = \omega_2$, a complete analytical solution is possible. Since the COM degrees of freedom separate, this solution is a trivial extension of Ref. [2]. Nonetheless, along with the general analysis of the previous section, it provides a physical picture for weak interaction between the COM and the relative degrees of freedom.

5.1. Identical frequencies

For $\omega_1 = \omega_2 = \omega$, the COM and relative coordinates separate, $H = H_{\text{rel}} + H_{\text{COM}}$, with

$$H_{\text{rel}} = \frac{\mathbf{p}^2}{2\mu} + \frac{1}{2} \mu \omega^2 \mathbf{r}_\perp^2 + V(\mathbf{r}), \quad H_{\text{COM}} = \frac{\mathbf{P}^2}{2M} + \frac{1}{2} M \omega^2 \mathbf{R}_\perp^2. \quad (60)$$

In this case, we can consider the two-particle system being (asymptotically) in the ground state of the decoupled COM Hamiltonian, and just solve the relative problem [2, 3]. Moreover, with $f(t) = \coth(\omega t)$ and $g(t) = \sinh^{-1}(\omega t)$, the Green's function (58) simplifies to

$$G_t(\mathbf{R}_\perp, 0; \mathbf{R}'_\perp, 0) = \sqrt{\frac{\mu}{2\pi t}} \frac{\beta(1-\beta)}{\pi a_M^2} \frac{e^{-\omega t}}{1 - e^{-2\omega t}} \sum_{n,m} e^{-\omega \epsilon_{n,m} t} \frac{1}{a_M^2} \psi_{n,m} \left(\frac{\mathbf{R}_\perp}{a_M} \right) \bar{\psi}_{n,m} \left(\frac{\mathbf{R}'_\perp}{a_M} \right). \quad (61)$$

In this case, $|n, m\rangle$ is an eigenstate of the decoupled Hamiltonian H_{COM} , and describes the COM motion also for finite \mathbf{r} . Moreover, $a_M = (M\omega)^{-1/2}$ and $a_\mu = a_M/(\beta(1-\beta)) = (\mu\omega)^{-1/2}$ are the characteristic lengths associated with H_{COM} and H_{rel} , respectively. Inserting Eq. (61) into Eq. (22) and rescaling t by 2ω , we obtain

$$\zeta_E = \sum_{n,m} \frac{|n, m\rangle\langle n, m|}{4\pi a_\mu} \int_0^\infty \frac{dt}{(\pi t)^{1/2}} \left(\frac{e^{-\Omega_{n,m}(E)t}}{1 - e^{-t}} - \frac{1}{t} \right), \quad (62)$$

with $\Omega_{n,m}(E) = (1 + \epsilon_{n,m} - E/\omega)/2$. The integral on the rhs of Eq. (62) is related to the integral representation of the Hurvitz zeta function $\zeta(1/2, \Omega_{n,m})$ [5, 10].

5.1.1. Bound states The condition given in Eq. (15) for a bound state with transverse configuration $|n, m\rangle$ translates into

$$\zeta \left(\frac{1}{2}, \Omega_{n,m} \right) = -\frac{a_\mu}{a}. \quad (63)$$

The zeta function is monotonic, and has the asymptotic scaling behavior

$$\zeta \left(\frac{1}{2}, \Omega \ll 1 \right) \approx \Omega^{-1/2}, \quad \zeta \left(\frac{1}{2}, \Omega \gg 1 \right) \approx -2\sqrt{\Omega}. \quad (64)$$

Inverting Eq. (63), we recover the bound-state energy found in Ref. [3]. The corresponding result is plotted in Fig. 1. As an immediate consequence of the decoupling of the COM degrees of freedom, the ϵ_λ -fold degenerate energies corresponding to excited transverse configurations follow from the COM transverse ground state by a shift along the ordinate in steps of ω . This is indicated by the dotted curves in Fig. 1. Notice that for energies above $E_0 = 2\omega$, corresponding to $E_B = 2\omega\Omega_{0,0}(E) < 0$, there exists an open channel, but the solutions associated with COM excited states are orthogonal to it. For this reason, the relevant condition for a bound state to exist with transverse configuration $|n, m\rangle$ is $\Omega_{n,m}(E) > 0$. From the scaling behaviors in Eq. (64), we find the limiting behaviors of the energy of the bound state at $|a_\mu/a| \ll 1$ as

$$\begin{aligned} E_{B,n,m} &\approx \frac{1}{2\mu a^2} \quad \text{for } a > 0, \\ E_{B,n,m} &\approx \frac{2a^2}{\mu a_\mu^4} \quad \text{for } a < 0, \end{aligned} \quad (65)$$

see Eqs. (27) and (36), with $c = \sqrt{\pi}a_\mu$ and $E_{B,n,m} = \omega\Omega_{n,m}$. Hence, in this highly degenerate case, there is exactly one bound state for each transverse configuration and each scattering length a .

5.1.2. Scattering states In order to identify resonant bound states of the closed channel, and the corresponding zero-momentum CIR, we subtract the contribution of the lowest-energy scattering channel in Eq. (62), and obtain

$$\begin{aligned}\tilde{\zeta}_E &= \zeta_E - \frac{|0,0\rangle\langle 0,0|}{4\pi a_\mu} \int_0^\infty \frac{dt}{(\pi t)^{1/2}} e^{-\Omega_0(E)t} \\ &= \sum_{n,m} \frac{|n,m\rangle\langle n,m|}{4\pi a_\mu} \zeta(1/2, \tilde{\Omega}_{n,m}(E)),\end{aligned}\quad (66)$$

with $\tilde{\Omega}_{0,0}(E) = \Omega_{0,0}(E) + 1$ and $\tilde{\Omega}_{n,m}(E) = \Omega_{n,m}(E)$ for $n + |m| > 0$. Hence the curve corresponding to the COM ground state is shifted vertically by 2ω and coincides with the curve corresponding to the excited states $|1,0\rangle$, $|0,2\rangle$ and $|0,-2\rangle$. Moreover, the coupling condition in Eq. (54) becomes $\langle 0,0|n,m\rangle \neq 0$, and is fulfilled only for $n = m = 0$. Though there are in principle infinitely many closed-channel bound states with energy 2ω (one for each curve), only one scattering resonance exists, since only one of them is coupled to the incoming scattering wave. Inserting Eq. (66) into Eq. (46) we recover for the 1D interaction strength g_{1D} the well known result [2]

$$g_{1D} = 2\omega a_\mu \left(\frac{a_\mu}{a} - \mathcal{C} \right)^{-1}. \quad (67)$$

5.1.3. Physical picture for the weakly interacting case When $\omega_1 \neq \omega_2$ but $\omega_1 \approx \omega_2$, a weak coupling to the COM degrees of freedom is generated, with two important consequences: (i) the degeneracies of the bound-state energies are lifted, and (ii) the coupling to the other higher-lying bound states is non-zero. Since the operators $\tilde{\zeta}_E$ and ζ_E commute with the z -component L_z of the angular momentum, the bound states are still labeled by the quantum numbers $\{n, m\}$. As far as the scattering solutions are concerned, the incoming wave is coupled only to states with angular momentum quantum number $m = 0$. Since $\langle 0,0|\tilde{\zeta}_E|0,0\rangle \approx \langle 1,0|\tilde{\zeta}_E|1,0\rangle$, a small off-diagonal element $\langle 0,0|\tilde{\zeta}_E|1,0\rangle$ is sufficient to couple the bound state with $\{n, m\} = \{1, 0\}$ to the incoming wave, yielding an additional CIR. As far as bound states are concerned, solutions with $E > E_0$ and $m = 0$ leak into the open channel, and cannot be regarded as localized bound states. Hence, for $|a_\mu/a| \gg 1$ and $a < 0$, there is only one bound state with zero angular momentum. In the opposite dimer limit, however, we encounter many dimer bound states.

5.2. The case $\omega_1 \neq \omega_2$: Relation to experiments

The case $\omega_1 \neq \omega_2$ is relevant for experiments involving two different atom species trapped in magnetic or optical traps [11, 12, 13]. For instance, in optical traps the confining potential depends on the detuning $\Delta = \omega_{\text{las}} - hc/\lambda$ of the laser frequency ω_{las} from the characteristic frequency hc/λ associated with the optical transition $ns \rightarrow np$, and is therefore different for two different atom species. This conclusion also applies to magnetic traps if the atoms are confined in hyperfine states with different projection of the magnetic moment along the magnetic field. As a concrete example, let us consider

a mixture of Bosonic ^{87}Rb atoms and Fermionic ^{40}K atoms. Sympathetic cooling has allowed to create an ultracold mixture of these two elements. By loading such a gas into a dipole trap and sweeping an external magnetic field, it has been possible [13] to identify three heteronuclear Feshbach resonances and to measure the 3D interspecies scattering length $a = -14$ nm. It seems feasible to tune the magnetic field near a Feshbach resonance and to observe the interspecies CIR. It is hence very interesting to know how many of them can be expected and to study their locations.

The confining potential for a neutral atom in a standing optical wave $\mathbf{E}(\mathbf{r}, t) = \mathbf{E}_0(\mathbf{r})\text{Re}[\exp(-i\omega_{\text{las}}t)]$ is $V_{\text{conf}}(\mathbf{r}) = -(\varepsilon_0/4)\alpha'\mathbf{E}_0^2(\mathbf{r})$, where $\alpha' = -e^2/(2m_e\omega_{\text{las}}\varepsilon_0\Delta)$ is the real part of the polarizability [14]. Let us consider a red-detuned laser field corresponding to $\Delta < 0$ and $\alpha' > 0$. In this configuration, the atoms are trapped around the maximum of the electric field. For a mixture of two species, each species experiences its own detuning Δ_K (Δ_{Rb}) given by the two transition wavelengths $\lambda_K = 767$ nm and $\lambda_{\text{Rb}} = 780$ nm. Within a parabolic approximation for the potential around its minimum, the ratio $\omega_K/\omega_{\text{Rb}}$ of trap frequencies for K and Rb atoms becomes

$$\frac{\omega_K}{\omega_{\text{Rb}}} = \left(\frac{\Delta_{\text{Rb}}}{\Delta_K} \frac{m_{\text{Rb}}}{m_K} \right)^{1/2}. \quad (68)$$

Let us estimate this ratio for typical parameters. In order to suppress spontaneous emission, we assume an average detuning of $\Delta = (\Delta_K + \Delta_{\text{Rb}})/2 = -0.1\omega_{\text{las}}$, yielding $\omega_{\text{las}} = 5hc(\lambda_K^{-1} + \lambda_{\text{Rb}}^{-1})/11$ and $\Delta_{\text{Rb}}/\Delta_K = (5\lambda_K^{-1} - 6\lambda_{\text{Rb}}^{-1})/(5\lambda_{\text{Rb}}^{-1} - 6\lambda_K^{-1}) = 0.84$. Taking also into account the mass ratio $m_{\text{Rb}}/m_K = 87/40$, we have $\omega_K/\omega_{\text{Rb}} = 1.35$, indicating a substantial coupling of COM and relative degrees of freedom.

Using Eq. (58), we can project the Green's function $G_t(\mathbf{R}_{\perp}, 0; \mathbf{R}'_{\perp}, 0)$ on the appropriate basis defined in Eq. (31) and then compute numerically $\tilde{\zeta}_E$ by performing the imaginary-time integration, see Appendix B. Then $\tilde{\zeta}_{E_0}$ can be diagonalized, and the effective interspecies 1D interaction constant $g_{1\text{D}}$ follows according to Eq. (46). The results are shown in the upper viewgraph of Fig. 2 in terms of the characteristic length $a_{\mu} = \sqrt{2/(\mu(\omega_K + \omega_{\text{Rb}}))}$. We find two resonances, indicating that the discussion of Sec. 5.1.3 applies to this particular case. In order to illustrate the interpretation of the CIR in terms of Feshbach-type resonances with bound states of the closed channels, we also plot in the lower viewgraph of Fig. 2 the dimensionless binding energy $\Omega = 2(E - \omega_K + \omega_{\text{Rb}})/(\omega_K + \omega_{\text{Rb}})$ of the corresponding bound state. As expected, the resonances occur at those values of a_{μ}/a for which the energy of the bound state of the closed channels coincides with the continuum threshold of the open channel.

6. Non-parabolic confining potentials

Describing the potential created by an optical or a magnetic guide as parabolic is to some extent a simplification which has to be verified. In fact, even though the lower-energy transverse states can rather well be approximated by the eigenfunctions of a 2D harmonic oscillator, in every real trap the confinement is to some degree non-parabolic. For resonant scattering, we expect to have a virtual occupation of many non-parabolic

transverse states. As a consequence, the location of the CIR will be slightly moved, and new resonances could be created. This can already be seen from an analysis similar to the one in Sec. 5.1.3 for small non-parabolic corrections. In order to tackle the problem quantitatively, a full numerical treatment is required since no analytical expression for the Green's function is in general available, in contrast to Sec. 5.

As an example, we consider the small non-parabolicity due to the presence of a longitudinal magnetic bias field B_z in a magnetic waveguide containing a single-species gas. This is necessary to avoid Majorana spin flips [15] and the subsequent escape of atoms out of the trap. A magnetic trapping potential is formed according to $V_{\text{conf}}(\mathbf{x}) = \mu_m |\mathbf{B}(\mathbf{x})|$, where $\mathbf{B}(\mathbf{x})$ is the applied magnetic field and $\mu_m = m_F g_F \mu_B$, with m_F being the magnetic quantum number of the atom in the hyperfine state $|F, m_F\rangle$, g_F the Landé factor and μ_B the Bohr magneton. Assuming that apart from the longitudinal bias field, the remaining magnetic fields create a parabolic and isotropic confinement in the transverse direction, the total confinement is given by

$$\chi V_{\text{conf}}(\mathbf{x}) = \sqrt{1 + 2\chi(x^2 + y^2)}, \quad (69)$$

where we have scaled energy in units of the parabolic trapping frequency ω and length in units of $a_\mu = (\mu\omega)^{-1/2}$. The parameter $\chi = \omega/(\mu_m B_z)$ is related to the Majorana spin flip rate Γ_{loss} [15]. The 1D effective interaction strength g_{1D} can be calculated following our general approach. We compute $\tilde{\zeta}_{E_0}$ numerically as outlined in Appendix B. The results are shown in Fig. 3 for $\chi = 0.067$, which corresponds to $\Gamma_{\text{loss}} = 10^{-6}\omega$. We find two resonances reflecting the cylindrical symmetry of the potential (69) and the weakness of non-parabolic corrections. The degeneracy of the parabolic case (shown in Fig. 3) is lifted and the original CIR is split into two nearby resonances. As expected, the effect of the non-parabolic transverse states shows up only in the deep resonant region, making the parabolic solution a very good approximation away from the resonant region. In turn, this requires a good experimental resolution in order to observe the two CIR.

7. Conclusions

To conclude, we have presented the general solution for two-body s-wave scattering in a two-component ultracold atom gas longitudinally confined to one dimension by an arbitrary trapping potential. The underlying key property is that the center-of-mass and the relative degrees of freedom of the two-particle problem do not decouple, as it is the case for a one-component gas and a pure parabolic confinement. Thus, no reduction to an effective single-particle problem is possible and the full coupled system has to be solved. In the framework of the pseudopotential approach, we derive the energy of the bound state when all transverse channels are closed. Simple analytical results were obtained in the limiting cases of the dimer as well as the BCS limit. Moreover, scattering solutions have been obtained when just one transverse channel is open. The effective 1D interaction constant g_{1D} can be calculated after diagonalizing a reduced Green's function. This can be achieved analytically for the special case of parabolic

confinement, where the well-known confinement-induced resonance is recovered. For a two-component gas, as well as for a non-parabolic confinement, more than one CIR occur, which reflect the symmetry properties of the confining potential. These findings were illustrated by applying our formalism to experimentally relevant questions. We are confident that once the CIR has been verified experimentally, also the effects of a non-parabolic trapping potential will be discerned.

Acknowledgments

We thank A. Gogolin and A. Görlitz for discussions. This work has been supported by the DFG-SFB/TR 12.

Appendix A: Short-time Green's function

In this Appendix, we illustrate how to expand the Green's function

$$G_t(\mathbf{X}; \mathbf{X}') = \langle \mathbf{X} | \exp[-(K(\mathbf{\Pi}) + U(\mathbf{X}))t] | \mathbf{X}' \rangle \quad (70)$$

with respect to t yielding the expression in Eq. (23) for $G_t(\mathbf{R}_\perp, 0; \mathbf{R}'_\perp, 0)$. In order to simplify the notation, we have introduced the five-dimensional vectors $\mathbf{X} = \{\mathbf{R}_\perp, \mathbf{r}\}$ and $\mathbf{\Pi} = \{\mathbf{P}_\perp, \mathbf{p}\}$ and the functions $K(\mathbf{\Pi}) = \mathbf{P}_\perp^2/2M + \mathbf{p}^2/2\mu$ and $U(\mathbf{X}) = V_1(\mathbf{R}_\perp + \mu\mathbf{r}_\perp/m_1) + V_2(\mathbf{R}_\perp - \mu\mathbf{r}_\perp/m_2)$ for the kinetic and the potential energy, respectively. First, we expand the Green's function around the free solution given by

$$\langle \mathbf{X} | \exp[-K(\mathbf{\Pi})t] | \mathbf{X}' \rangle = \frac{M}{2\pi t} \exp\left[-\frac{(\mathbf{R}_\perp - \mathbf{R}'_\perp)^2 M}{2t}\right] \left(\frac{\mu}{2\pi t}\right)^{3/2} \exp\left[-\frac{(\mathbf{r} - \mathbf{r}')^2 \mu}{2t}\right]. \quad (71)$$

In order to justify such an expansion, note that for $t \rightarrow 0^+$

$$\langle \mathbf{X} | K(\mathbf{\Pi}) \exp[-K(\mathbf{\Pi})t] | \mathbf{X}' \rangle = -\frac{d}{dt} \langle \mathbf{X} | \exp[-K(\mathbf{\Pi})t] | \mathbf{X}' \rangle \propto \delta(\mathbf{X} - \mathbf{X}') \frac{1}{t}, \quad (72)$$

whereas

$$\langle \mathbf{X} | U(\mathbf{X}) \exp[-K(\mathbf{\Pi})t] | \mathbf{X}' \rangle = U(\mathbf{X}) \langle \mathbf{X} | \exp[-K(\mathbf{\Pi})t] | \mathbf{X}' \rangle \propto U(\mathbf{X}) \delta(\mathbf{X} - \mathbf{X}'). \quad (73)$$

Since the kinetic energy in Eq. (72) diverges whereas the potential energy in Eq. (73) remains finite, the latter can be regarded as a small perturbation. This expansion yields

$$G_t(\mathbf{X}; \mathbf{X}') \simeq (1 - tU(\mathbf{X})) \langle \mathbf{X} | \exp[-K(\mathbf{\Pi})t] | \mathbf{X}' \rangle. \quad (74)$$

Let us now set $\mathbf{X}_0 = \{\mathbf{R}'_\perp, 0\}$ in Eq. (71) and expand with respect to t :

$$\begin{aligned} & \langle \mathbf{R}_\perp, 0 | \exp[-K(\mathbf{\Pi})t] | \mathbf{R}'_\perp, 0 \rangle \\ &= \left(\frac{\mu}{2\pi t}\right)^{3/2} \frac{M}{2\pi t} \exp\left[-\frac{(\mathbf{R}_\perp - \mathbf{R}'_\perp)^2 M}{2t}\right] \\ &= \left(\frac{\mu}{2\pi t}\right)^{3/2} \int \frac{d^2 \mathbf{P}_\perp}{(2\pi)^2} \exp[i\mathbf{P}_\perp \cdot (\mathbf{R}_\perp - \mathbf{R}'_\perp) - \frac{\mathbf{P}_\perp^2}{2M} t] \\ &\simeq \left(\frac{\mu}{2\pi t}\right)^{3/2} \int \frac{d^2 \mathbf{P}_\perp}{(2\pi)^2} \left(1 - \frac{\mathbf{P}_\perp^2}{2M} t\right) \exp[i\mathbf{P}_\perp \cdot (\mathbf{R}_\perp - \mathbf{R}'_\perp)] \\ &= \left(\frac{\mu}{2\pi t}\right)^{3/2} \left(\delta(\mathbf{R}_\perp - \mathbf{R}'_\perp) - t \frac{\mathbf{P}_\perp^2}{2M}\right). \end{aligned}$$

In the last line, the operator \mathbf{P}_\perp^2 stands for $(2\pi)^{-2} \int d^2\mathbf{P}_\perp \langle \mathbf{R}_\perp | \mathbf{P}_\perp \rangle \mathbf{P}_\perp^2 \langle \mathbf{P}_\perp | \mathbf{R}'_\perp \rangle$. Inserting \mathbf{X}_0 into Eq. (74), we finally obtain Eq. (23).

Appendix B: Evaluation of the operators ζ_E and $\tilde{\zeta}_E$

In this Appendix, we outline the evaluation of the kernels ζ_E and $\tilde{\zeta}_E$ given in Eqs. (22) and (30), respectively.

B1: Parabolic confinement, $\omega_1 \neq \omega_2$

First, let us consider the special case of parabolic confinement, but the two species may experience different trap frequencies. For this confinement, the Green's function $G_t(\mathbf{R}_\perp, 0; \mathbf{R}'_\perp, 0)$ is given in Eq. (58). The first step is to project this operator onto the appropriate orthonormal basis $\{|j\rangle\}$ defined in Eq. (31). Note that this definition allows an arbitrary choice of the basis, apart from properly fixing the vector $|0\rangle$. One possibility is introduced in Eq. (56). This is a natural option because it reflects the cylindrical symmetry of the problem. However, this choice would not permit further analytical progress. For this reason, we employ an alternative basis defined by

$$\langle \mathbf{R}_\perp | j \rangle = \langle \mathbf{R}_\perp | n_x, n_y \rangle = \frac{1}{a_M} \psi_{n_x} \left(\frac{x}{a_M} \right) \psi_{n_y} \left(\frac{y}{a_M} \right), \quad (75)$$

where $\psi_n(x)$ is the eigenfunction for the 1D oscillator in dimensionless units, $\psi_n(x) = (\sqrt{\pi} 2^{n_x} n!)^{-1/2} \exp(-x^2/2) H_n(x)$, with $H_n(x)$ being Hermite polynomials. Note that the x and y directions factorize in the Green's function (58), allowing to perform the x and y integrals separately. For convenience, we introduce dimensionless coordinates $x \rightarrow x/a_M$ and find

$$\begin{aligned} [G(t)]_{\mathbf{n}, \mathbf{m}} &= \langle n_x, n_y | G_t(\mathbf{R}_\perp, 0; \mathbf{R}'_\perp, 0) | m_x, m_y \rangle \\ &= \sqrt{\frac{\mu}{2\pi t}} \frac{\beta(1-\beta)}{\pi^2 a_M^2} \frac{e^{-\omega_1 t}}{1 - e^{-2\omega_1 t}} \frac{e^{-\omega_2 t}}{1 - e^{-2\omega_2 t}} [F(t)]_{n_x, m_x} [F(t)]_{n_y, m_y} \end{aligned} \quad (76)$$

with

$$[F(t)]_{n, m} = \int dx dx' \bar{\psi}_n(x) \exp \left[-\frac{x^2 + x'^2}{2} f(t) + xx' g(t) \right] \psi_m(x'). \quad (77)$$

The functions $f(t)$ and $g(t)$ are defined in Eq. (59). We perform the first integration by using the identity [10]

$$\int dz e^{-(z-z')^2} H_n(\alpha z) = \pi^{1/2} (1 - \alpha^2)^{n/2} H_n \left(\frac{\alpha z'}{(1 - \alpha^2)^{1/2}} \right), \quad (78)$$

with $\alpha = \alpha(t) = [(1 + f(t))/2]^{-1/2}$, $z = x/\alpha(t)$ and $z' = g(t)\alpha(t)x'/2$, yielding

$$\begin{aligned} [F(t)]_{n, m} &= (2^{n+m} m! n!)^{-1/2} \alpha(t) (1 - \alpha(t)^2)^{n/2} \\ &\times \int dx' \exp \left[-x'^2 \left(\alpha^{-2}(t) - \frac{g(t)\alpha^2(t)}{4} \right) \right] H_n \left(\frac{g(t)\alpha^2(t)}{2(1 - \alpha^2(t))^{1/2}} x' \right) H_m(x'). \end{aligned} \quad (79)$$

By substituting Eq. (76) together with Eq. (79) into ζ_E defined in Eq. (22), and by introducing the dimensionless time $t' = \sqrt{t(\omega_1 + \omega_2)}$, we get

$$[\zeta_E]_{\mathbf{n},\mathbf{m}} = \frac{1}{4\pi a_\mu} \int_0^\infty dt' \left\{ A h_E(t') \left[F\left(\frac{t'^2}{\omega_1 + \omega_2}\right) \right]_{m_x, n_x} \right. \\ \left. \times \left[F\left(\frac{t'^2}{\omega_1 + \omega_2}\right) \right]_{m_y, n_y} - \frac{2}{\pi^{1/2} t'^2} \delta_{\mathbf{n},\mathbf{m}} \right\} \quad (80)$$

with the dimensionless parameter $A = 2\pi^{-3/2}\beta(1-\beta)a_\mu^2/a_M^2$ and

$$h_E(t') = \exp\left[-\frac{(\omega_1 + \omega_2 - E)t'^2}{\omega_1 + \omega_2}\right] \left(1 - \exp\left[-\frac{2\omega_1 t'^2}{\omega_1 + \omega_2}\right]\right)^{-1} \\ \times \left(1 - \exp\left[-\frac{2\omega_2 t'^2}{\omega_1 + \omega_2}\right]\right)^{-1}. \quad (81)$$

It is now possible to evaluate the matrix elements of $[\zeta_E]_{\mathbf{n},\mathbf{m}}$ by numerically computing the double integrals in Eq. (80). Note that the integrand does not suffer from any singularity due to the rescaling of the integration variable. Moreover, the convergence of the x' integral (79) is exponentially fast. The first term in the integrand of the t' integral decays exponentially at large times. Hence for large times, only the second term yields a contribution, where the integration can be performed analytically in this region. For the case of interspecies scattering of Rb and K in an optical trap, all the parameters entering in $A, h_E(t)$ and $[F(t)]_{n,m}$ can be expressed in terms of the ratios $m_{\text{Rb}}/m_{\text{K}}$ and $\Delta_{\text{Rb}}/\Delta_{\text{K}}$. The generalization to determine $\tilde{\zeta}_E$ is straightforward and not detailed further.

B2: Non-parabolic confinement

A numerical evaluation of the operator ζ_E and $\tilde{\zeta}_E$ is less straightforward when the Green's function $G_t(\mathbf{R}_\perp, 0; \mathbf{R}'_\perp, 0)$ cannot be computed analytically. In this case, $G_t(\mathbf{R}_\perp, 0; \mathbf{R}'_\perp, 0)$ should be computed by numerical diagonalization of the $H_{\perp,i}$ and inserting their eigenvalues and eigenfunctions into Eq. (20). For large t , this is feasible because only a small number of eigenfunctions contribute to the sum. However, for $t \rightarrow 0$, the number of eigenvectors required to cancel the divergence in Eq. (22) quickly proliferates. This practical limitation can fortunately be circumvented by the following trick. Let us formally rewrite Eq. (22) as

$$\zeta_E(\mathbf{R}_\perp, \mathbf{R}'_\perp) = \int_0^\infty \frac{dt}{2\mu} \left\{ e^{Et} [G_t(\mathbf{R}_\perp, 0; \mathbf{R}'_\perp, 0) - G_t^0(\mathbf{R}_\perp, 0; \mathbf{R}'_\perp, 0)] \right. \\ \left. + e^{Et} G_t^0(\mathbf{R}_\perp, 0; \mathbf{R}'_\perp, 0) - \left(\frac{\mu}{2\pi t}\right)^{3/2} \delta(\mathbf{R}_\perp - \mathbf{R}'_\perp) \right\} \\ = \int_0^\infty \frac{dt}{2\mu} e^{Et} [G_t(\mathbf{R}_\perp, 0; \mathbf{R}'_\perp, 0) - G_t^0(\mathbf{R}_\perp, 0; \mathbf{R}'_\perp, 0)] \\ + \zeta_E^0(\mathbf{R}_\perp, \mathbf{R}'_\perp), \quad (82)$$

where $G_t^0(\mathbf{R}_\perp, 0; \mathbf{R}'_\perp, 0)$ and $\zeta_E^0(\mathbf{R}_\perp, \mathbf{R}'_\perp)$ are the Green's function and the integral kernel, respectively, for an arbitrary reference confining potential $V_0(\mathbf{x}_\perp)$. If $G_t^0(\mathbf{R}_\perp, 0; \mathbf{R}'_\perp, 0)$ is known analytically, we can deal with $\zeta_E^0(\mathbf{R}_\perp, \mathbf{R}'_\perp)$ as in the previous section. For confining potentials close to the parabolic case, we choose a parabolic $V_0(\mathbf{x}_\perp)$.

Regarding Eq. (82), we proceed as follows. We restrict the infinite-dimensional Hilbert space to the \mathcal{N} lowest eigenstates of the potential $V_0(\mathbf{x}_\perp)$, and diagonalize the original Hamiltonian in this \mathcal{N} -dimensional Hilbert space. With the eigenfunctions at hand, the Green's function can be computed using Eq. (20). Then, the sum in Eq. (20) is exchanged with the t -integration and the latter is performed. Next, we project the Green's function onto a known single-particle basis $\{|m\rangle\}$. To achieve numerical convergence, we increase the Hilbert space dimension \mathcal{N} until the result does not change anymore. We emphasize that the overall result converges to the exact result although obviously not all the single-particle states used in computing the Green's function are reliable on very long distances (comparable to the numerical system size) because higher-lying energy states are increasingly inaccurate. Nevertheless, the central part (in position space) of the eigenfunctions – which corresponds to the kinetic energy and does not feel the confinement – is accurate enough to cancel the divergence stemming from the kinetic part. In order to compute the scattering solution, we compute $\tilde{\zeta}_{E_0}$ with an analogous procedure, diagonalize $\tilde{\zeta}_{E_0}$ numerically, and insert the result into Eq. (46). For the non-parabolic confinement in Sec. 6, a parabolic $V_0(\mathbf{x}_\perp)$ is appropriate. In this case, we use for $\{|m\rangle\}$ the orthonormal basis defined in Eq. (56). Then ζ_E^0 is diagonal and given by Eq. (66).

References

- [1] D.S. Petrov, D.M. Gangardt, and G.V. Shlyapnikov 2004 *J. Phys. IV France* **116** 5
- [2] M. Olshanii 1998 *Phys. Rev. Lett.* **81** 938
- [3] T. Bergeman, M.G. Moore, and M. Olshanii 2003 *Phys. Rev. Lett.* **91** 163201
- [4] M. G. Moore, T. Bergemann, and M. Olshanii 2004 *J. Phys. IV (France)* **116** 69
- [5] C. Mora, R. Egger, A.O. Gogolin, and A. Komnik 2004 *Phys. Rev. Lett.* **93** 170403; C. Mora, R. Egger, and A.O. Gogolin 2005 *Phys. Rev. A* **71** 052705
- [6] C. Mora, A. Komnik, R. Egger, and A.O. Gogolin, cond-mat/0501641
- [7] H. Moritz, T. Stöferle, K. Günter, M. Köhl, and T. Esslinger 2005 *Phys. Rev. Lett.* **94** 210401
- [8] V. Peano, M. Thorwart, A. Kasper, and R. Egger *submitted to Appl. Phys. B., see also quant-ph/0505210*
- [9] E. Timmermans, P. Tommasini, M. Hussein, and A. Kerman 1999 *Phys. Rep.* **315** 199
- [10] I. S. Gradshteyn and I.M. Ryzhik 1965 *Tables of Integrals, Series and Products* (London: Academic Press)
- [11] G. Modugno, G. Ferrari, G. Roati, R. J. Brecha, A. Simoni, and M. Inguscio 2001 *Science* **294** 1320
- [12] Z. Hadzibabic, C. A. Stan, K. Dieckmann, S. Gupta, M. W. Zwierlein, A. Görlitz, and W. Ketterle 2002 *Phys. Rev. Lett.* **88** 160401
- [13] S. Inouye, J. Goldwin, M. L. Olsen, C. Ticknor, J. L. Bohn, and D. S. Jin 2004 *Phys. Rev. Lett.* **93** 183201
- [14] G. Grynberg and C. Robilliard 2001 *Phys. Rep.* **355** 335
- [15] C. V. Sukumar and D. M. Brink 1997 *Phys. Rev. A* **56** 2451

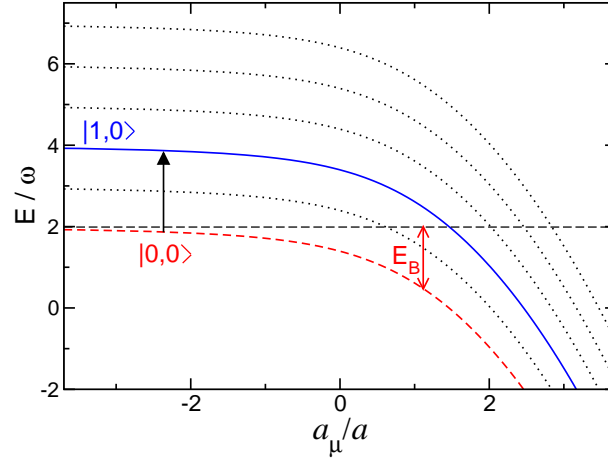


Figure 1. Bound state energies E as a function of a_μ/a for harmonic confinement with equal frequency ω for both atoms. The dashed red curve indicates the bound state energy of the ground state $|0,0\rangle$. Its binding energy E_B is given by the distance to the horizontal dashed line indicating the continuum threshold for the open channel. The blue curve marks the bound state energy of the virtual bound state relevant for the low-energy scattering. It is obtained by a vertical shift of the ground-state energy by 2ω , and coincides with the three-fold degenerate bound-state energy indicated as solid curve. The black dotted curves give the bound-state energies of the excited transverse states, obtained by a vertical shift of the ground-state result.

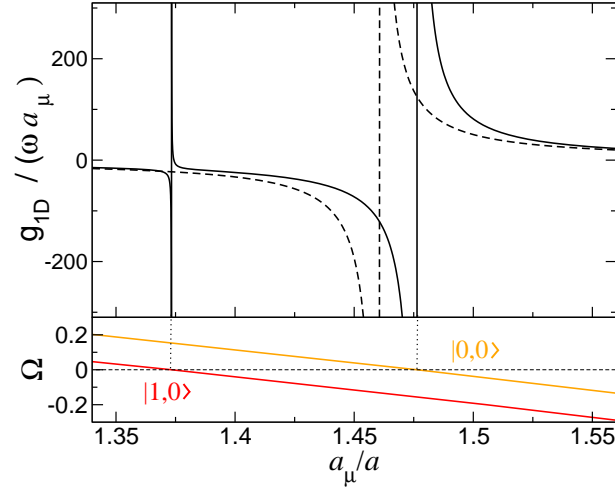


Figure 2. Upper viewgraph: CIR in the effective interspecies 1D interaction constant g_{1D} as a function of a_μ/a . We consider a two-component atom gas of ^{40}K and ^{87}Rb , with average detuning $\Delta = -0.1\omega_{\text{las}}$ (solid line). For comparison, we also show the result for the case when the two species experience the same trap frequency (dashed line). Lower viewgraph: Dimensionless binding energy Ω for the two states $|0,0\rangle$ and $|1,0\rangle$.

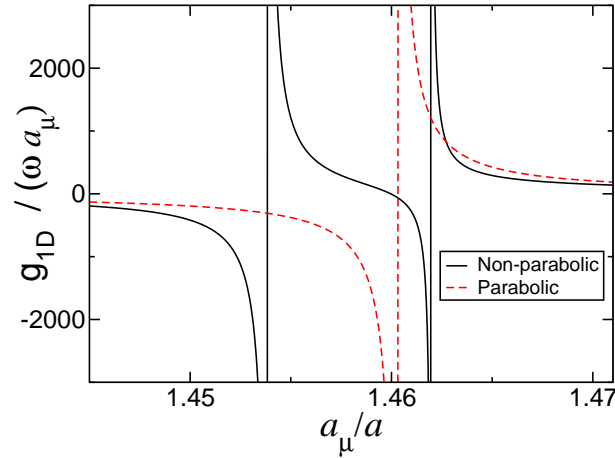


Figure 3. 1D effective interaction strength g_{1D} for the non-parabolic potential of Eq. (69) (black solid line) for $\chi = 0.067$ corresponding to $\Gamma_{\text{loss}} = 10^{-6}\omega$. For comparison, the parabolic case is also shown (red dashed line).